Utrecht University

Faculteit Bètawetenschappen

Exploring In on InAs(111)A as a platform for quantum simulation

Bachelor Thesis Natuur- en Sterrenkunde

Margriet van Riggelen

Thomas Gardenier MSc Daily Supervisor
Dr. Ingmar Swart Project Supervisor
Debye Institute for Nanomaterials Science

April 15, 2020

Abstract

Artificial lattices are of great interest for simulation of complex quantum systems. Rearranging CO molecules on Cu(111) has shown to be a very reliable method to construct them but energy broadening in the measurements posed a problem. We expect to solve this by using a different electronic platform: we are using the scanning tunneling microscope to manipulate In adatoms on an InAs(111)A-(2 x 2) surface. Samples grown using the Liquid Encapsulated Czochralski (LEC) technique with a top layer grown by molecular-beam epitaxy (MBE) were shown to exhibit less defects and are therefore more suitable for this experiment than LEC-grown samples without an MBE-grown layer. To increase the amount of adatoms for manipulation, In was deposited from a crucible onto the sample by heating the crucible via electron bombardment. The kinetic energy of the electrons plays an important role: 1 keV kinetic energy resulted in single In atoms on the surface, while 2 keV kinetic energy resulted in small clusters of In atoms. Vertical manipulation of In adatoms was performed while $I(z)$ traces were recorded. Individual In adatoms were picked up from and deposited onto the substrate with atomic precision. Challenges lie in finding out when and why holes in the surface are made when picking up an atom and how to prevent depositing clusters of In atoms. We constructed an In_{10} and an In_6 chain using vertical manipulation. The lowest energy state of the In_6 chain is reported to be located at -0.131 V. We did not detect a clear signal of this particle-in-a-box like state. To do this, the vertical manipulation method should be further optimized and more artificial lattices should be assembled. Quantum simulators constructed in this manner promise to be of great value in the field of quantum computing.

Contents

1 Introduction **1**

2 Theory **2**
2.1 Scanning Tunneling Microscopy . . . 2
2.2 Two-dimensional electron gas . . . 2
2.3 Vertical manipulation . . . 3

3 Methods **5**

4 Results and discussion **6**
4.1 Sample preparation . . . 6
4.1.1 LEC-grown samples versus samples with an MBE-grown top layer . . . 6
4.1.2 Evaporation of indium . . . 6
4.2 Vertical manipulation . . . 7
4.2.1 Picking up In adatoms . . . 7
4.2.2 Deposition of In adatoms . . . 9
4.3 Chains of In adatoms . . . 10
4.3.1 Ten atom chain . . . 10
4.3.2 Six atom chain . . . 11

5 Conclusions and outlook **13**

6 Acknowledgements **14**

1 Introduction

The idea of engineering lattices using the manipulation of individual atoms is as old as the famous lecture by Richard Feynman given at the annual American Physical Society meeting in 1959. 'Why dig in the ground to find minerals with a certain specific impurity density when we should be able to tailor perfect lattices ourselves?' [1]. This principle of engineering artificial lattices is what drives a lot of recent research and can be realized in very diverse systems, such as cold atoms [2, 3], trapped ions [4], superconducting circuits [5], optical lattices [6] and electronic lattices [7, 8]. These artificial lattices can be used to perform quantum simulation, i.e. using some controllable quantum system (the artificial lattice) to describe a less controllable or accessible quantum system (e.g. a molecule) [9]. Quantum simulators in the form of artificial lattices are ideally suited for testing theoretical models, because all relevant symmetries and interactions can be controlled using, e.g., atom manipulation with a scanning tunneling microscope.

In the case of electronic lattices as quantum simulators, two different concepts can be applied, based on whether the interactions between the surface adsorbates (atoms or molecules) are localized or delocalized. If the interactions are localized, the electronic structure of the lattices is described by the tight-binding model. Structures assembled from closely bound atoms adsorbed on a surface, or lattices of coupled vacancies, are well described using this model. Experimental realization takes the form of, for example, coupled Cu atoms on a Cu(111) surface [10] or coupled Cl vacancies on CuCl/Cu(111) [11]. However, if the interactions are delocalized, the electronic structure of the lattices is best described by the nearly free electron model. This is the case when the lattice is constructed by patterning the two-dimensional electron gas with periodic scattering potentials [7, 12, 13]. Patterning the two-dimensional electron gas of the Cu(111) surface with CO molecules is common, because the manipulation of the CO molecules is very reliable. In this system, the CO molecules pose a repulsive barrier for the surface state electrons of the copper. By trapping the electronic waves between CO molecules, an artificial atom can be created. However, this configuration has a downside. Cu(111) is a metal, i.e. it does not have a band gap. The surface state is located in a quasi-gap which exists due to the termination of the periodicity of the crystal [14]. When a surface state electron is scattered, it can end up in one of the bulk states, causing coupling between the surface state and the bulk states. This leads to energy broadening exhibited in the differential conductance spectra above artificial lattices, which is an undesirable limitation to the resolution of the measurements.

The solution to this problem would be using a semiconductor instead of a metal, because semiconductors do have a band gap. In this experiment, we are following Fölsch et al. [15] in using In adatoms on a InAs(111)A surface as a platform. They have shown that the energy resolution using this platform is of an order of magnitude better than for CO on Cu(111) [16]. With this in mind, we are exploring the possibilities of constructing artificial lattices on the InAs(111)A-(2 x 2) surface and this thesis reports on our progress so far.

After introducing the theory behind the experiments and reporting the specifics of the methods used (sections 2 and 3), this thesis will describe the results on optimizing sample preparation (section 4.1). The sample preparation consists of choosing the type of substrate and ensuring there is a sufficient amount of In adatoms to manipulate by evaporation of In onto the surface. Next, the results of the vertical manipulation of the adatoms are discussed (section 4.2). Using this method, we built an In_{10} chain and an In_6 chain, the results of which will be presented and discussed in section 4.3. In section 5, our conclusions and recommendations for further research are offered.

2 Theory

In this section, a theoretical framework is given behind the conducted experiments. Firstly, the scanning tunneling microscope is introduced, the device that embodies Feynman's visions. Subsequently, the surface we worked with is looked into with more detail, also explaining the origin of the two-dimensional electron gas. Finally, the theory behind atom manipulation is explained.

2.1 Scanning Tunneling Microscopy

In this experiment, the scanning tunneling microscope (STM) is used to image the samples and to manipulate the In adatoms. In the following section a qualitative description of the working of the STM is given. The interested reader can find more details in for example Ref. [17] or [18].

The STM was invented by Binnig and Rohrer in 1981/1982 [19]. They received the Nobel prize for it in 1986 [17]. A schematic of the STM is shown in figure 1. The STM makes use of an atomically sharp metal tip as a probe, which can be used to image the surface. A voltage difference between the tip and the sample is realized by applying a bias voltage V to the sample and keeping the tip grounded. The tip is brought close to the sample until a current I flows. The current is formed by electrons tunneling through the potential barrier of the vacuum from the tip to the sample or vice versa, and can be detected at tip-sample distances in the order of $d = 0.5$-1 nm [14]. At a constant bias voltage, the magnitude of the tunneling current I depends exponentially on the tip-sample distance d and is therefore used to measure and control d. A 20% change in the tunneling current corresponds to a change in the tip-sample distance of $\Delta z = 0.01$ nm [18]. Imaging the surface is performed by moving the tip in x- and y-direction along the surface in constant-current mode, in which I is maintained at a reference value using a feedback loop. This means that when the tip is coming near a step edge of height Δz on the surface for example, the current will increase. To maintain a constant current the tip-sample distance is increased by Δz. Recording d while scanning an area of the surface gives the topography of this area.

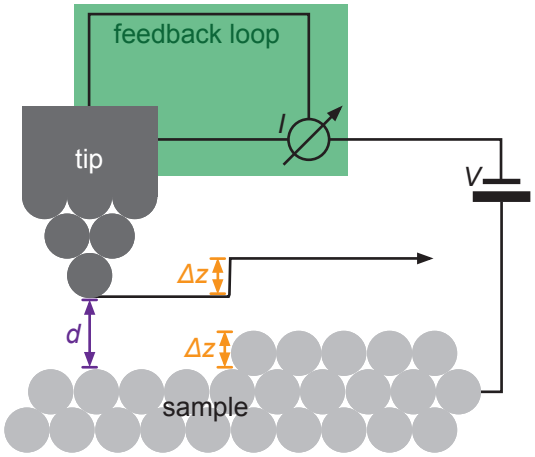

Figure 1: Schematic of the STM. A bias voltage V is applied between the tip and the sample. If the tip is in the vicinity of the sample, a tunneling current I flows, which corresponds to a certain tip-sample distance d. When imaging the tip moves along the surface. The feedback loop maintains a constant current, e.g. changing d with Δz when scanning over a step edge with that same height Δz.

2.2 Two-dimensional electron gas

The electronic structure of artificial lattices can be described by two different models, the tight-binding model and the nearly free electron model. For CO molecules on Cu(111) and for In adatoms on InAs(111)A, the nearly free electron approach is applicable, because the adsorbates confine and restructure the two-dimensional electron gas (2DEG). In this section the origin of this 2DEG is explained. Figure 2a shows the

geometry of the InAs(111)A-(2 x 2) surface which we worked with. The 'A' type of the InAs(111) surface terminates with a layer of In atoms. One quarter of a monolayer of these In atoms is missing, yielding a (2 x 2) In vacancy reconstruction with a unit cell as indicated in figure 2a. The cubic InAs lattice constant is $a_0 = 0.606$ nm, which results in a (2 x 2) vacancy spacing of $a' = a_0\sqrt{2} = 0.857$ nm [20, 21]. The energy band diagram of the material is shown in figure 2b. Positively charged In adatoms located at the In vacancy sites donate an electron to the conduction band and due to the poor screening of the surface charge-induced electric field by the low concentration of free carriers in the semiconductor, this leads to an accumulation of negative charge in the region just below the surface (the accumulation layer) [22]. At the InAs(111)A surface, the conduction band minimum (CBM) is pulled down as far as 0.2 eV below the Fermi level (E_F) of the substrate. This leads to a 2DEG at the surface [16, 23].

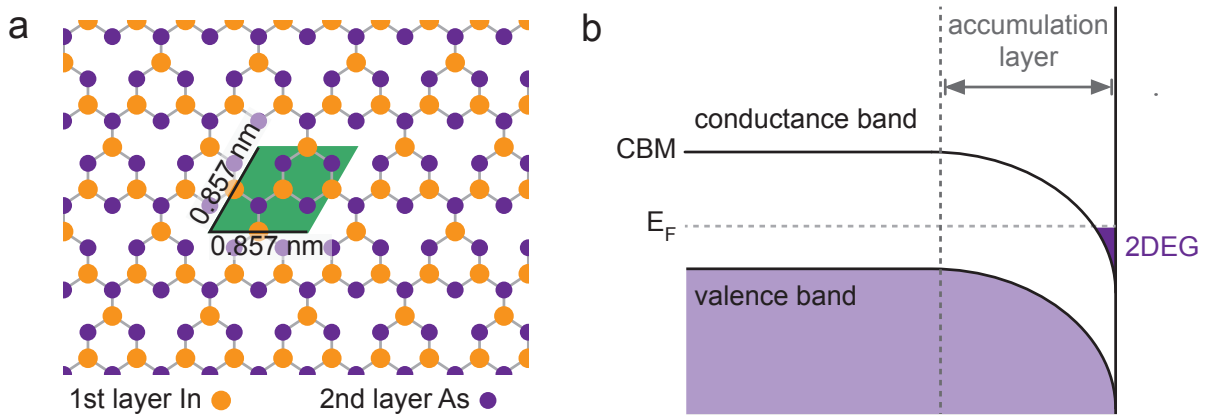

Figure 2: (a) Stick-and-ball model of the first two atomic layers of the InAs(111)A-(2 x 2) surface. The topmost layer (In atoms) is represented by orange circles and the second layer (As atoms) by purple circles. The unit cell is indicated by the green parallelogram. The spacing of nearest-neighbour vacancies is $a' = 0.857$ nm. (b) Energy band diagram of the region near the InAs(111)A-(2 x 2) surface. In the accumulation layer, the conduction band minimum (CBM) is pulled below the Fermi level (E_F) and a two-dimensional electron gas (2DEG) arises, which is separated from the valence band electrons.

With CO on Cu(111), the CO molecules are patterned onto the 2DEG and serve as scattering centers. They can be used to form the boundaries of the box in the particle-in-a-box picture. New eigenstates $\Psi(E,x)$ form as a function of energy E and position x [12], i.e. an artificial atom is created. In contrast, the In adatoms on InAs(111)A do not serve as scattering centers but are attractive for the surface state electrons, creating a potential well. This results in local charge accumulation around the In adatoms which can be observed when imaging the sample with a positive sample bias: a halo of increased apparent height surrounds the In adatoms [24]. To create a similar particle-in-a-box picture as with CO on Cu(111), one places several In adatoms in a structure, for example a line, creating a bigger potential well and in this way an artificial atom. The relevant surface state arises predominantly from the unoccupied 6s atomic orbitals of the surface In atoms [15]. This state becomes quantized by the artificial atom. The resulting chain-confined states resemble the wave functions for a quantum particle in a box. These wave functions have n lobes and n-1 nodes with n the principal quantum number and can be visualized using scanning tunneling spectroscopy [16]. The artificial atoms can be assembled into larger artificial lattices in order to use them for quantum simulation.

2.3 Vertical manipulation

The manipulation of individual atoms was done first by Eigler and Schweizer in 1990. They manipulated Xe atoms on a Ni(110) surface to create a IBM logo [25]. Atom manipulation is based on the principle that there is a force between the tip and the atom, when approaching the tip close enough to the substrate. Two methods used for atom manipulation are illustrated in figure 3. In the case of lateral manipulation, the tip drags or pushes the atom along the surface. In this case, the force between the tip and the atom is strong

enough to overcome the surface diffusion barrier [14]. If, e.g., one would manipulate adatoms on a metal surface, there is an attractive force between the tip and the atom which makes the atom follow the lateral motion of the tip [12]. For vertical manipulation, the atom is transferred to the tip and redeposited on a different position on the substrate, using voltage pulses of opposite polarity.

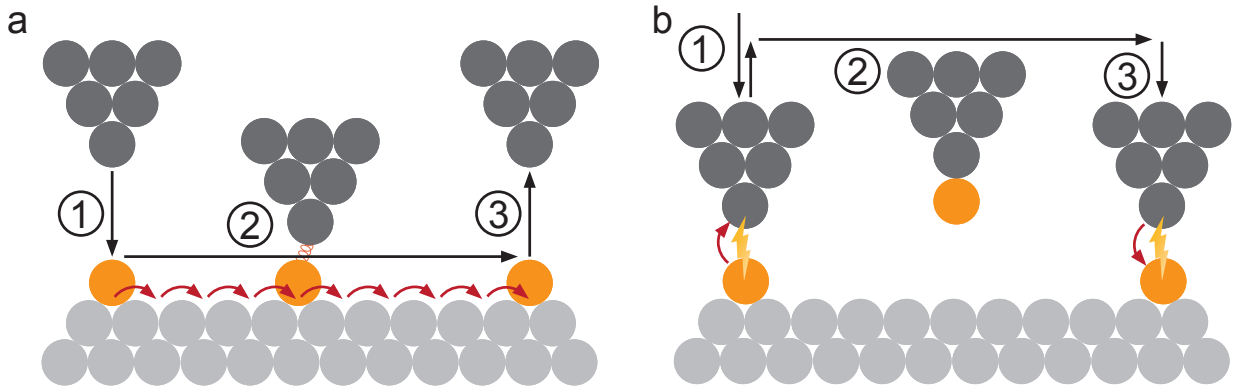

Figure 3: Schematic representations of atom manipulation. The tip is shown in dark grey, the substrate in light grey. The adatom to be manipulated is represented by the orange circles. The different steps are indicated by the encircled numbers. (a) Schematic of lateral manipulation. In the first step, the tip is approached to just above the adatom. Due to the force between the tip and the atom, the atom follows the tip while the tip moves laterally to the desired deposition spot (step 2). In the third step, the tip is retracted and the bond between the adatom and the tip is broken. (b) Schematic of vertical manipulation. In step one, the tip is approached towards the adatom and due to the voltage difference between the tip and the adatom the adatom transfers to the tip. The second step is retracting the tip with the adatom and moving it in x- and y-direction to the desired deposition spot. In the final step, the tip is approached again above a vacancy site while a negative bias voltage is applied. When the tip is brought close enough to the sample, the tip-sample transfer takes place.

In this thesis, the vertical manipulation procedure of Fölsch et al. [15] is followed. They report that In adatoms on InAs(111)A-(2 x 2) can be picked up by the STM tip applying a positive sample bias of >0.7 V and approaching the tip to the adatom. The current rises and subsequently drops, indicating the adatom transferring from the surface to the tip. For the tip-to-surface transfer, the tip is positioned above an In vacancy site and a negative sample bias of any magnitude is applied. The tip is approached until the short-range adhesive forces induce the tip-to-surface transfer [21]. Examples of $I(z)$ traces are shown in section 4.2.

3 Methods

The experiments were carried out with a low temperature STM, manufactured by Sigma Surface Science, now part of Scienta Omicron. The system is operated at a temperature of 4.5 K under ultrahigh vacuum (UHV), a pressure of $p = 10^{-11}$-10^{-9} mbar. The experiments were done on two types of samples. The first type is a one side polished, 500 ± 25 µm thick undoped n-type InAs wafer, purchased from WaferTech Ltd with orientation (111)A ± 0.1° and a (2 x 2) In vacancy reconstruction. It is grown by the Liquid Encapsulated Czochralski (LEC) technique. This type of sample is cleaned by repeated cycles of sputtering and annealing, based on a method described by Olsson et al. [23]. For the sputtering, Argon gas is leaked into the preparation chamber up to a pressure of $p = 8.5 \text{ x } 10^{-6}$ mbar. The Ar is ionized and the sample is bombarded with Ar^+ ions for 15 minutes. After removing the top layers of the sample in this way, the sample is annealed for 30 minutes at 750 K.

For the second type of sample the standard LEC-grown sample as described above was used as substrate for an undoped 100 nm layer of InAs grown by molecular-beam epitaxy (MBE) with the same surface reconstruction as the LEC-grown sample. The MBE step was executed by The Institute of Electronics, Microelectronics and Nanotechnology in Lille, France. Directly after the MBE growth, the surface was capped with an amorphous layer of arsenic and transferred under ambient conditions to the UHV system of the STM. The As capping layer was removed by annealing the sample at a temperature of 520 K.

The tip used was an obliquely cut Pt/Ir wire covered in In at the apex. To create an atomically sharp tip apex, tip conditioning was performed by current pulsing at sample bias voltages varying from 1 to 10 V and by tip-surface contact. The voltage pulses result in the agglomeration of indium at the tip apex [21]. dI/dV spectra were obtained using scanning tunneling spectroscopy (STS). The STS measurements were performed in constant height mode using a lock-in amplifier which modulates the sample bias with a 5 mV peak-to-peak amplitude and a frequency of 973 Hz. For the In evaporation onto the sample, a crucible was filled with In pellets and heated via electron bombardment using a wire filament. The process was controlled by tuning the voltage over the filament and the In flux, measured by a flux sensor. Details are described in section 4.1.2.

4 Results and discussion

This section presents the results we obtained of the investigation of the electronic platform formed by In adatoms on the InAs(111)A-(2 x 2) surface. Before atom manipulation was performed, the sample was prepared (section 4.1). Subsequently, the vertical manipulation method was looked into (section 4.2) and finally we constructed two artificial lattices, the results of which will be discussed in section 4.3.

4.1 Sample preparation

To build artificial lattices, the surface should contain as few defects and impurities as possible. At the same time, a sufficient number of adatoms should be available for manipulation. To determine which of the two types of InAs(111)A surface is best suited for quantum simulation experiments, we first investigate the purity of both substrates. Subsequently, we report the results on evaporating additional In atoms onto the surface.

4.1.1 LEC-grown samples versus samples with an MBE-grown top layer

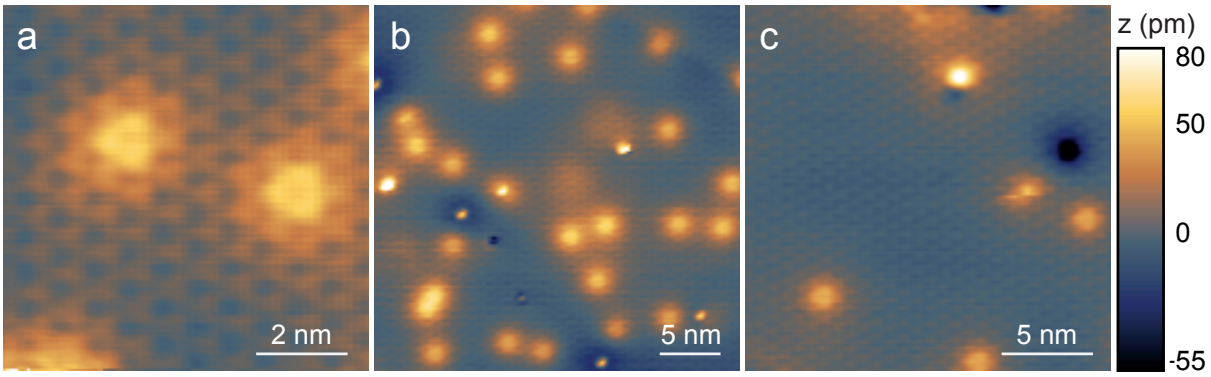

Figure 4: STM topographs (10 nA, 0.5 V) of the surfaces of InAs(111)A-(2 x 2) samples. (a) STM topograph (8 nm x 8 nm) of features with a diameter of approximately 3 nm and an apparent height of approximately 4 pm. (b) STM topograph (30 nm x 30 nm) of the surface of the LEC-grown sample. The image shows approximately 24 of the features as described in (a). (c) STM topograph (20 nm x 20 nm) of the surface of a sample with an MBE-grown top layer. The image shows approximately four features as described in (a).

Figure 4 shows STM topographs of the two types of InAs(111)A samples we have investigated. In figures 4a/b, LEC-grown samples are shown. In figure 4c, a sample with an MBE-grown top layer is shown. One can clearly see triangular shaped features with a diameter of approximately 3 nm and an apparent height of approximately 4 pm. Prolonging the Ar sputtering time does not lower the number of these defects. The density of these features on the LEC-grown samples is approximately $0.04/\text{nm}^2$, an order of magnitude larger than on the samples with the MBE-grown top layer, on which the density is approximately $0.004/\text{nm}^2$. We tentatively assign these defects to chemical impurities in the InAs(111)A wafer. Due to the amount of these defects, we consider the samples with the MBE-grown top layer more suitable for the construction of artificial lattices.

4.1.2 Evaporation of indium

Figure 5 shows STM topographs of the InAs(111)A surface onto which In is deposited. One can see individual In adatoms (encircled in green) as well as clusters of In adatoms (encircled in red). Evaporation was performed by heating a crucible filled with In pellets via electron bombardment. We found that the kinetic energy of the electrons plays an important role: a kinetic energy of $T = 2$ keV resulted in predominantly clusters of In atoms, $T = 1$ keV resulted in predominantly individual adatoms. We presume this difference is due to the fact that at higher kinetic energy not only individual In atoms evaporate from the crucible but also small In clusters. Since individual adatoms are more convenient for atom manipulation, we consider evaporation with $T = 1$ keV more suitable for this experiment.

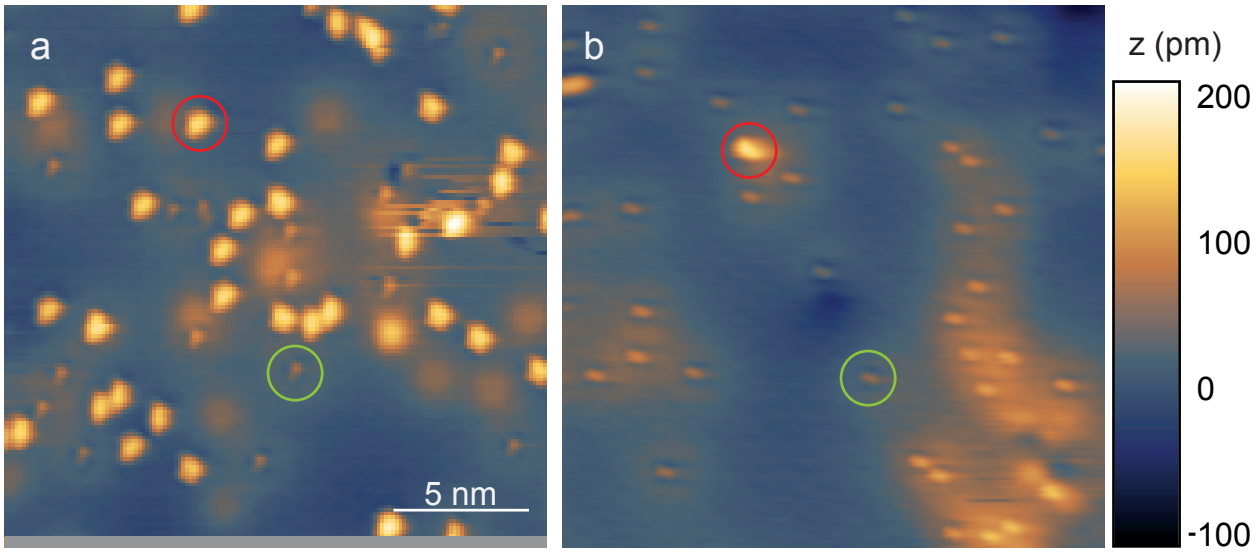

Figure 5: Comparison of evaporation of In with a kinetic energy of 2 keV and evaporation of In with a kinetic energy of 1 keV. Scale bar applies to both images. Examples of In clusters (less suitable for manipulation) are encircled in red, individual In adatoms (more suitable for manipulation) are encircled in green. (a) STM topograph (10 nA, 0.5 V, 20 nm x 20 nm) of InAs sample after evaporation with a kinetic energy of 2 keV (voltage over filament 2.0 kV, for 10 s with a flux of 10 nA). The image shows approximately 19 individual In adatoms and 34 In clusters. (b) STM topograph (10 nA, 0.5 V, 20 nm x 20 nm) of InAs sample after evaporation with a kinetic energy of 1 keV (voltage over filament 1.0 kV, for 20 s with a flux of 5 nA). The image shows approximately 37 individual In adatoms and two In clusters.

4.2 Vertical manipulation

It has been reported that In adatoms can be picked up from and placed onto the InAs(111)A-(2 x 2) surface with atomic scale accuracy, using vertical manipulation (see section 2.3). To optimize this procedure, we recorded the current I while inducing tip-to-sample or sample-to-tip transfers. 104 $I(z)$ traces of successful transfers were acquired in this manner. In the following, the surface-to-tip transfers will be discussed, after which we will turn our attention to the tip-to-surface transfers.

4.2.1 Picking up In adatoms

We followed the procedure described by Fölsch et al. [15]. The tip is positioned above the adatom to be manipulated at a tip-sample separation corresponding to set point parameters of $I = 1$ nA and $V = 0.5$ V. The feedback loop is interrupted, after which the bias voltage is set to $V = 1.25$ V. The tip is brought close to the surface until the transfer takes place.

68 $I(z)$ traces were recorded of successful surface-to-tip transfers. Representative $I(z)$ curves are shown in figure 6e/f. Imaging the same area after the $I(z)$ curve was recorded, reveals that the adatom above which the $I(z)$ trace was recorded was picked up, see figure 6a-d. In 67% of the cases the current increases for decreasing tip-sample separation, until a sudden drop, indicating the transfer. This typical curve is reported as well by Yang et al. [21] and examples are shown in figure 6e. The sudden decrease in the current indicating the sample-to-tip transfer is indicated by the arrow. After this event the current increases again for decreasing tip-sample distance. There are no sudden jumps in the current in the reverse direction, i.e. when the tip-sample distance increases. The tip-sample separation at which the sudden drop in the current took place varies from -0.06 nm to -0.25 nm measured from set point (1 nA, 0.5 V). The current that is reached before the sudden drop varies from 0.5 µA to 7 µA. In the remaining cases (33%) the atom was successfully picked up, but the current did not show a sudden drop as described above. The trace showed either no sudden jumps at all or various sudden changes (see figure 6f).

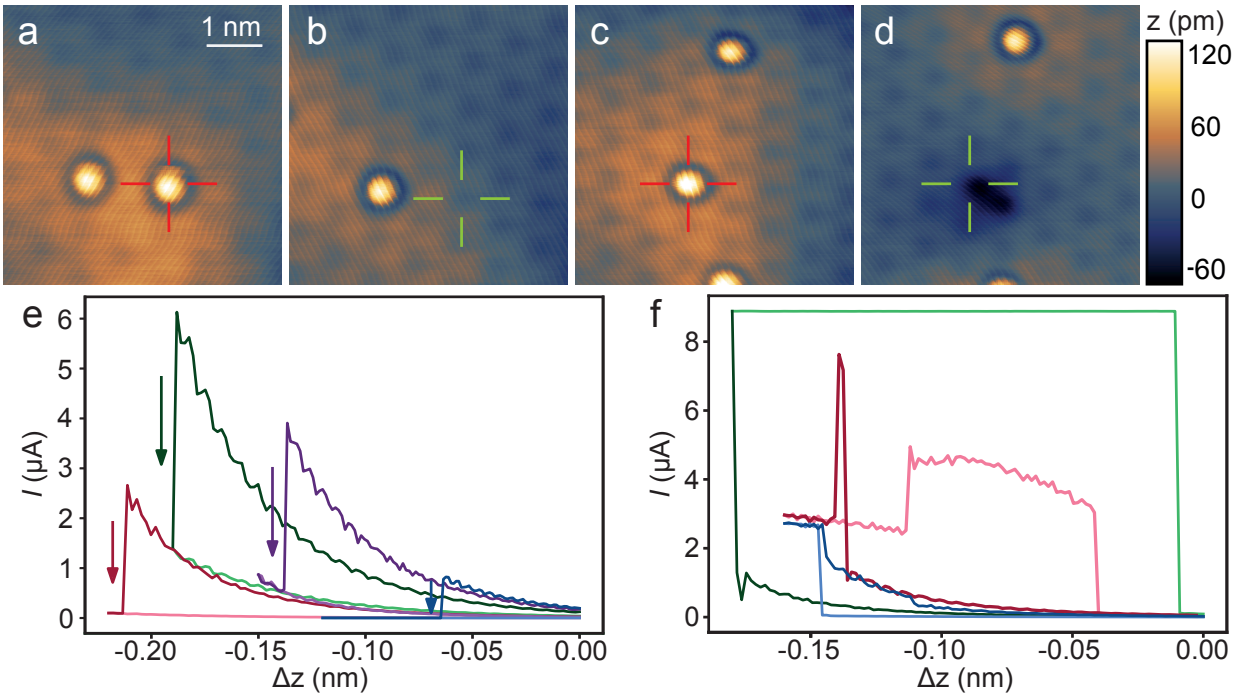

Figure 6: (a-d) STM topographs (10 nA, 0.5 V, 5 nm x 5 nm) showing the picking up of an atom. Scale bar applies to all images. (a)/(c) Above the atoms highlighted with the red cross marks the tip was positioned at a tip-sample separation corresponding to set point parameters of I = 1 nA and V = 0.5 V. The feedback loop was interrupted, after which a bias voltage of V = 1.25 V was applied. The tip was approached while recording the tunneling current I. (b)/(d) After changes in the current the tip was retracted to the tip-sample separation corresponding to the set point parameters and the bias was changed back to V = 0.5 V. The feedback loop was enabled again and the area was scanned. The green cross marks indicate the positions from which the atoms were transferred. (e)/(f) $I(z)$ traces of surface-to-tip transfers. The dark colored traces correspond to decreasing tip-sample separation and the light colored traces correspond to increasing tip-sample separation. (e) Typical $I(z)$ traces of surface-to-tip transfers. The current increases for decreasing tip-sample separation, until a sudden drop, indicated by the arrows. After this event the current increases again for decreasing tip-sample distance. There are no sudden jumps in the reverse direction. (f) $I(z)$ traces of surface-to-tip transfers that were less common than the typical traces in (e). The green trace shows a sudden increase at approximately Δz = -0.18 nm measured from set point (1 nA, 0.5 V) to saturation (above I = 8.88 μA).

In more than a third of the cases of a successful surface-to-tip transfer we found that a hole was made in the surface, as shown in figure 6d. The holes appear as depressions in the surface and we have not yet found a procedure to restore the original surface after a hole is created. The $I(z)$ curves corresponding to a surface-to-tip transfer leaving a hole, were less often of the typical kind, namely 44% compared to 80% in the cases no hole was made. The tip-sample distance range in which the transfer took place when making a hole was similar, just as the range of values that the current reached, to when no hole was made. This makes it difficult to know in advance whether the picking up of the atom was successful, i.e. no hole was made, or not. In 20% of the cases a hole was made however, the current had saturated (>8.88 μA), the trace would then be similar to the green trace in figure 6f. Saturation did not occur for the cases no hole was created.

To create less holes, more research should be done on when a hole is made. We presume it is related to how far the tip approaches, since tip-surface contact might create holes. This is however not substantiated yet by the data analyzed for this thesis. A different cause of the holes could be unsuitability of the tip apex for picking up atoms, which could be further analyzed by qualifying the shape of the tip apex before attempting to pick up an atom. It could also be the case that some adatoms are more strongly bound to the surface than others. Picking up the more strongly bound atoms could then result in making holes. If this is the case, we should investigate which atoms are better bound and why.

4.2.2 Deposition of In adatoms

To place an atom onto the surface, again the procedure by Fölsch et al. [15] was followed. The tip is positioned above a vacancy site of choice at tip-sample separation corresponding to set point parameters of I = 1 nA and V = 0.5 V. The feedback loop is interrupted, after which the voltage is set to V = -1 V. The tip is brought close to the surface and the tip-surface transfer of the atom takes place. In figure 7 representative $I(z)$ curves for tip-to-surface transfers are shown.

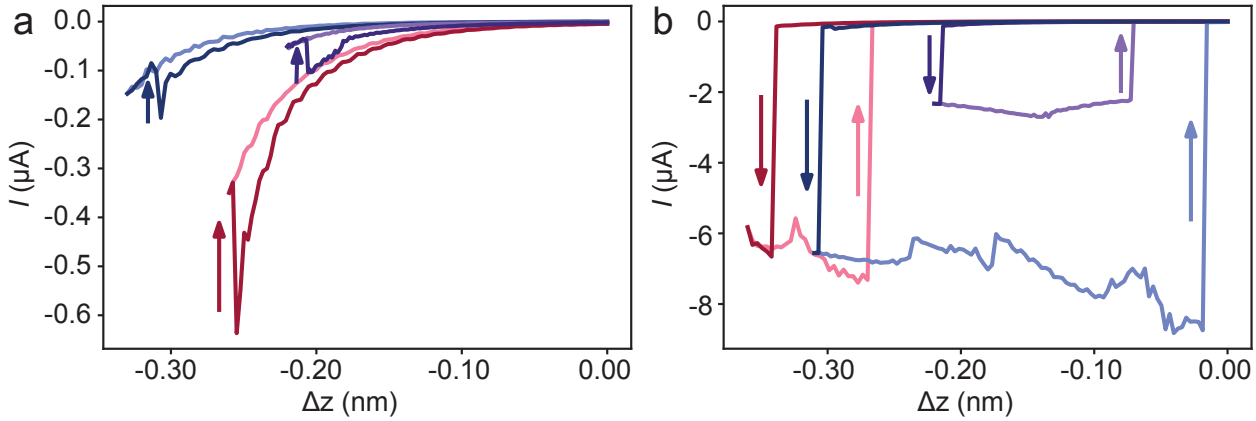

Figure 7: $I(z)$ traces of tip-to-surface transfers. The dark colored traces correspond to decreasing tip-sample distance and the light colored traces correspond to increasing tip-sample distance. The tip was positioned above a vacancy site at tip-sample separation corresponding to set point parameters of 1 nA and 0.5 V, after which the feedback loop was interrupted and the bias voltage was changed to -1 V. The tip is approached to the surface and after sudden changes in the current the tip was retracted to the distance corresponding to the set point parameters and the bias was changed back to 0.5 V. The feedback loop was enabled again and the area was scanned. (a) First type of trace which was acquired in 47% of the cases. The current decreases with decreasing tip-sample separation, until a sudden increase, indicated by the arrows. After this event the current decreased again for decreasing tip-sample separation. There are no sudden jumps in the reverse direction. (b) Second kind of trace which was acquired in 44% of the cases. The trace initially shows a sudden decrease of 2 μA to more than 8 μA, indicated by the dark colored arrows, after which it remains low even though the tip-sample distance increases, until a sudden increase of approximately the same magnitude, indicated by the light colored arrows.

36 $I(z)$ traces were recorded while placing an atom onto the surface. Representative curves are shown in figure 7. In 47% of the cases the current decreased with decreasing tip-sample separation, until a sudden increase, indicating the tip-to-surface transfer. After this event, the current decreased again for decreasing tip-sample distance. There were no sudden jumps in the current in the reverse direction, i.e. when the tip-sample distance increases. Examples of this type of curve are shown in figure 7a. The tip-sample distance at which the jump in the current occurs varies from -0.21 nm to -0.31 nm measured from set point (1 nA, 0.5 V). The lowest current reached before the jump varies from -0.1 μA to -0.6 μA. This kind of trace seems to represent the opposite process of the typical trace for surface-to-tip transfers as shown in figure 6e. In figure 7b, a different type of trace is shown which occurred in 44% of the cases. The trace initially shows a drop of 2 μA to more than 8 μA, after which it remains low even though the tip-sample separation was increasing, until a jump up of approximately the same magnitude as the drop down. The initial drop takes place at -0.16 nm to -0.34 nm and the jump back up occurs at distances varying from -0.02 nm to -0.27 nm, all measured from set point. In the remaining cases, the current did drop down but did not jump back up again.

For the tip-to-surface transfers, we encountered problems with reproducibility. Yang et al. [21] report a success rate of about 70% for the tip-to-surface transfers, while in the remaining cases In dimers or larger In clusters were deposited. We encountered this problem as well, in approximately half of the cases. Depositing too many atoms would not necessarily be a problem, except that our surface-to-tip procedure sometimes causes unrestorable holes as described above. These problems with reproducibility are the reason that the chains we built as described in section 4.3 have imperfections surrounding them. However, electronic features can still be measured on these chains and these measurements show good prospects for future research.

4.3 Chains of In adatoms

Using the method described in section 4.2, we built two chains of In adatoms, one In_{10} chain in the $[\bar{1}2\bar{1}]$ direction and one In_6 chain in the $[\bar{1}2\bar{1}]$ direction. As explained in section 2.2, a chain of ionized In adatoms represents an artificial atom that confines surface state electrons. The resulting particle-in-a-box wave functions can be visualized using dI/dV spectroscopy, in which the lobes should appear as regions of high differential conductance and the nodes as regions of low differential conductance.

4.3.1 Ten atom chain

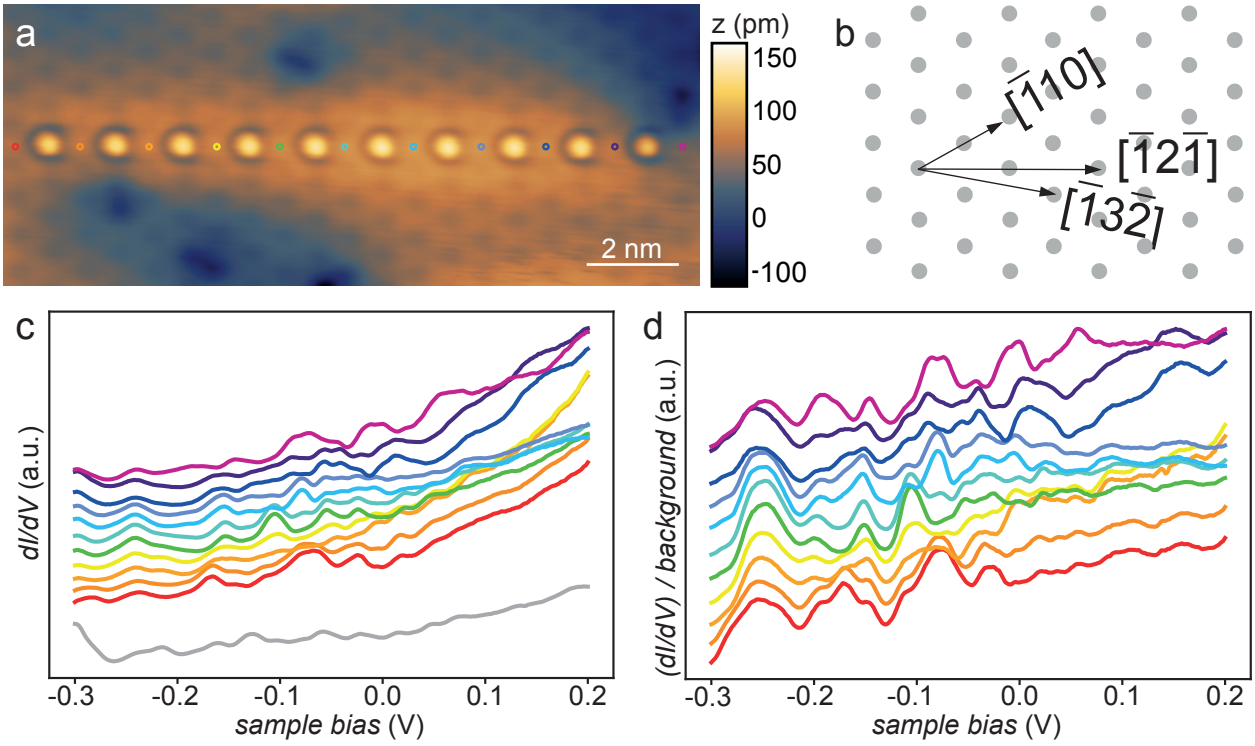

Figure 8: (a) STM topograph (10 nA, 0.5 V) of In_{10} chain in the $[\bar{1}2\bar{1}]$ direction assembled by atom manipulation. The depressions around the chain are due to imperfect surface-to-tip transfers of adatoms. The colored dots indicate where the dI/dV spectra in (c)/(d) were recorded. (b) Indication of the different in-plane directions for building chains of In adatoms on the vacancy sites of the InAs(111)A-(2 x 2) surface. (c) dI/dV spectra of the In_{10} chain (recorded at the positions indicated in (a), red spectrum corresponds red dot at the left in (a), orange spectrum to orange dot etc.). The spectra are shown with an offset for clarity. The grey spectrum corresponds to an average of 11 background spectra acquired on InAs. (d) dI/dV spectra as in (c), but divided by the average background.

Figure 8a shows an In_{10} chain in the $[\bar{1}2\bar{1}]$ direction as illustrated in figure 8b. The depressions around the chain are due to surface-to-tip transfers that left holes as described in paragraph 4.2. Two series of 11 dI/dV spectra were acquired just next to and in between the atoms of the chain. The locations at which the spectra were recorded are indicated by the colored dots in figure 8a. The two spectra at each location were similar which is a good indication of reproducibility of the results and led us to average the two spectra. The results are shown in figure 8c/d. The red spectrum in figure 8c/d corresponds to the red dot in 8a, the orange spectrum to the orange dot etc. The spectra are plotted with an offset for clarity of the features. 11 background spectra were acquired at the InAs surface and averaged. This average background is shown in grey in figure 8c. In figure 8d the spectra measured at the chain were divided by the average background in order to be able to identify which features in the dI/dV spectra are caused by the chain.

Ideally, we would see the features of a discrete ground state of the artificial atom that we made here. We would expect this ground state to have a high differential conductivity in the middle of the chain and a differential conductance one at the edges. The peaks in the turquoise and green spectra around -0.11 could be an indication of this ground state. However, multiple peaks are observed and no definite conclusions can be drawn from the results of this chain. This problem of multiple peaks could be due to a few different things. As mentioned before, the depressions around the chain could influence the results. It could also be the case that during the dI/dV measurements, the tip apex rearranged itself. Finally, other constructions of adatoms in the neighbourhood of this In_{10} chain could have influenced the measurements. A lot of improvements still can be made, it is nevertheless promising that reproducible features in the dI/dV spectra can be measured.

4.3.2 Six atom chain

Figure 9a shows a by vertical manipulation constructed In_6 chain in the $[\bar{1}10]$ direction as illustrated in figure 9b. Pan et al. [16] report that for the six atom chain one should be able to recognize the ground state (n=1) of the artificial atom at -131 mV. Their results are shown in figure 9c, the results for the measurements in the middle of the In_6 chain are indicated by the green curve. In order to reproduce these results, 65 dI/dV were acquired alongside the In_6 chain we built. The locations at which the spectra were acquired are indicated by the multicolored line in 9a. 30 background spectra were measured at the InAs surface and averaged.

The data obtained by registering the dI/dV spectra was processed in three different ways, shown in figure 9d-f. The dotted grey lines indicate where the ground state in the spectrum was reported. In figure 9d, the 65 dI/dV spectra were all divided by the background and separately shown in a contourplot. The regions of high differential conductance are indicated yellow and the regions of low differential conductance are blue. A feature that is notable is the horizontal blue region around the 55th spectrum (in the middle of the yellow part of the position indicating line). This is due to three spectra with lower values for the differential conductance, but similar features. This could be due to a temporarily changed tip apex or to the hole under the last atom. From the contourplot, it seems as if we have a peak rather around -0.095 V than at the expected -0.131 V.

In figure 9e/f five spectra on the left of the chain were averaged to create the blue curves, five spectra in the middle of the chain were averaged to create the green curves and five spectra at the right of the chain were averaged to create the yellow curves. We did not take the outermost spectra to obtain the average because from the results from Pan et al. [16] the impression is that the ground state is not visible at all at the outermost atoms. In figure 9e, the spectra are divided by the background, just as in the contourplot. The different curves are shifted such that their first data points have the same average value. This can be done because the set point values when disengaging the feedback loop should be the same for all curves. The first point of the yellow spectrum is ignored, since this was a point that does not correlate with the other points of the curve. What can be seen using this method of data processing is that the curves not only have comparable differential conductance values at the beginning but also at the end of the spectra, from about 0.1 V to 0.2 V. We note that the yellow curve has less recognizable peaks, which is due to the same spectra with lower values that created the blue region in the contourplot. In this figure, at -0.131 the differential conductance is clearly lower at the ends of the chain than in the middle, which could indicate the ground state.

In figure 9f, the dI/dV curves were divided by the corresponding I/V curves in order to normalize them, after which they were shifted in a similar manner as in 9e. The grey curve indicates the background. At -0.131 V there seems to be a depression in the curves rather than a peak, but this depression is even more distinct in the background. This results in the peak around -0.131 in 9e.

In conclusion, the features of the ground state are not as clear as we would expect based on the results presented by Pan et al. [16]. This could be due to several problems, of which the most prominent are discussed in section 4.3.1. The chain could also have drifted during the registration of the spectra. For the In_{10} chain as well as for the In_6 chain a problem of significance is the stability of the setup as a whole. At the In_{10} chain, only two series of 11 spectra could be acquired before the tip crashed into the sample causing an agglomeration of In on top of the chain. At the In_6 chain, attempts to map the differential conductance as a function of position resulted in a crash of the same kind. Stability should therefore be improved by tracing down and eliminating all kinds of noise.

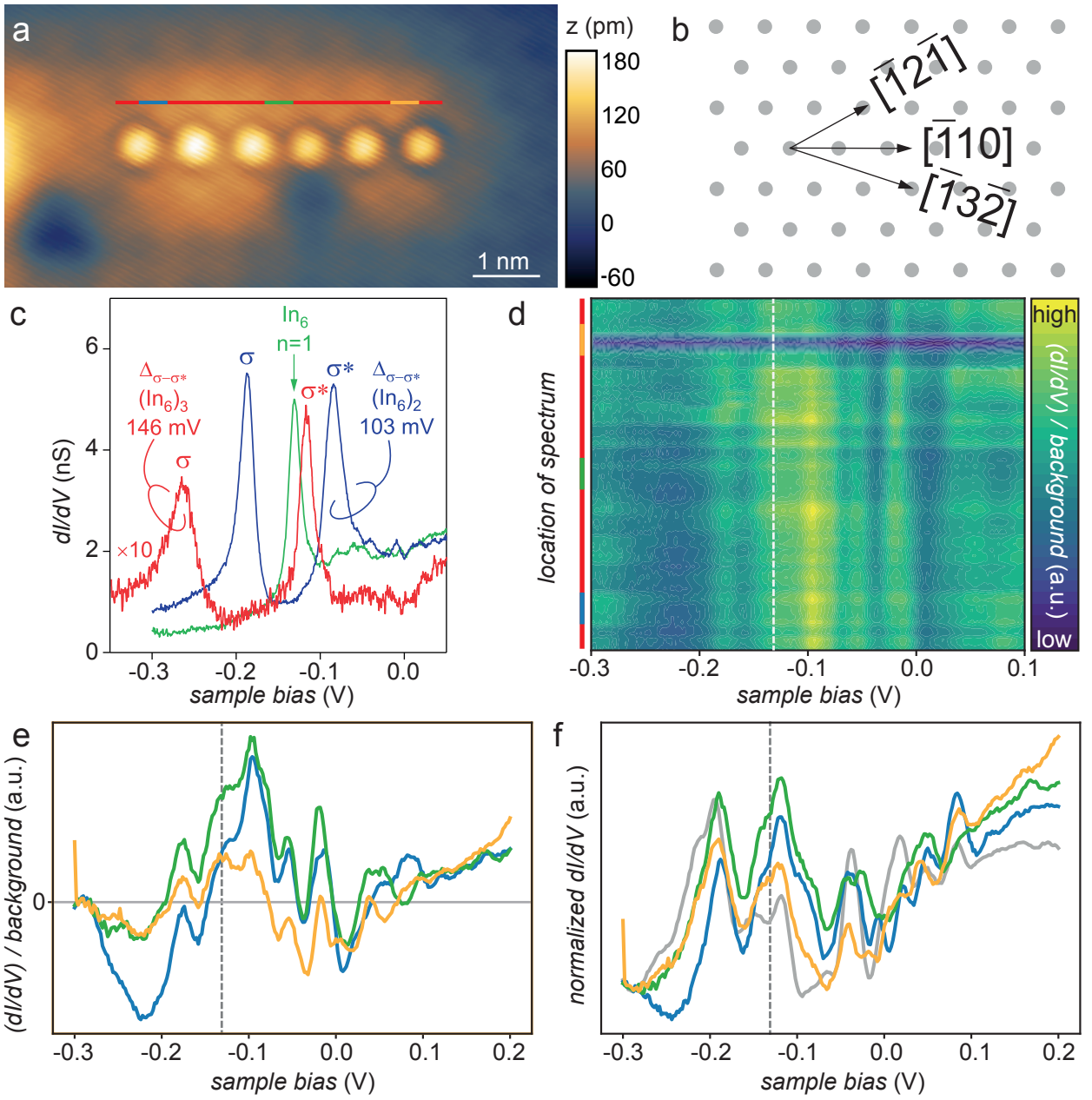

Figure 9: (a) STM topograph (10 nA, 0.5 V) of In_6 chain in the $[\bar{1}10]$ direction, assembled by atom manipulation. The depressions around the chain are due to imperfect surface-to-tip transfers of adatoms. On the multicolored line, 65 equally spaced dI/dV spectra were recorded. (b) Indication of the different in-plane directions for building chains of In adatoms on the vacancy sites of the InAs(111)A-(2 x 2) surface. (c) dI/dV spectrum of the discrete In_6 chain with the ground state (n=1) located at -131 mV in green. The red and blue curves are dI/dV spectra of $(In_6)_2$ and $(In_6)_3$ molecules. Panel adapted from Ref. [16]. (d) Contourplot of the (dI/dV)/background spectra. The vertical axis indicates where the spectrum is taken next to the chain, the colors correspond to the colors in (a). The dotted grey line indicates where the ground state in the spectra was reported to be. (e) Averaged dI/dV spectra from the left (blue curve), middle (green curve) and right side of the chain yellow curve. The colors correspond to the colors in (a). The spectra were divided by the background and shifted such that the first points had the same average value. (f) Averaged dI/dV spectra from the left (blue), middle (green) and the right (yellow) of the chain. The spectra were divided by the corresponding I/V curves in order to normalize them and shifted such that the first points had the same value.

5 Conclusions and outlook

We investigated the suitability of the InAs(111)A-(2 x 2) surface with In adatoms as an electronic platform for the construction of artificial atoms. LEC-grown samples with an MBE-grown top layer exhibit less defects and are therefore more suitable than the LEC-grown samples without the MBE-grown layer. To increase the amount of the adatoms for manipulation In was deposited onto the sample. We found that single In adatoms can be deposited from a crucible by heating the crucible via electron bombardment. The kinetic energy of the electrons plays an important role: 1 keV kinetic energy resulted in predominantly individual In atoms on the surface, while 2 keV kinetic energy resulted in predominantly small clusters of In atoms. Atomically precise vertical manipulation of In adatoms was performed, while $I(z)$ traces were recorded. When an atom was successfully picked up, in 67% of the cases the current showed a sudden drop of one to a few μA. For the remaining cases in which picking up an atom took place and for deposition of atoms onto the sample, various other traces were observed. Challenges lie in finding out when and why holes in the surface are made when picking up an atom and how to prevent depositing larger clusters of In atoms when attempting to deposit an individual atom. Despite these problems with reproducibility, we constructed an In_{10} and an In_6 chain using vertical manipulation. In literature, the lowest energy state of the In_6 chain was reported to be located at -0.131 V. We did not detect a clear signal of a particle-in-a-box like state. To do this, the manipulation method should be further optimized and the stability of the system should be improved. When artificial atoms can be constructed on InAs(111)A-(2 x 2) in a reliable manner, the structures can be extended to simulate various quantum states of matter. A possible direction for future exploration could be topologically non-trivial states, protected by the symmetries of the system [12]. This promises to be of great use in e.g. topological quantum computing [26].

6 Acknowledgements

I would like to thank Thomas for supervising me daily and his never ending patience in answering all of my questions and Ingmar for the helpful advice and fruitful discussions. I would like all of Team Kelder for helping me out with all kinds of problems, from ugly coding in Python to a headache, and for the fun we had.

References

[1] Feynman, R. P. (1960). There's Plenty of Room at the Bottom. *Engineering and Science*, *23*(5), 22–36.
[2] Bloch, I. (2005). Ultracold quantum gases in optical lattices. *Nature Physics*, *1*, 23–30.
[3] Bloch, I., Dalibard, J., & Nascimbène, S. (2012). Quantum simulations with ultracold quantum gases. *Nature Physics*, *8*(4), 267–276.
[4] Blatt, R., & Roos, C. F. (2012). Quantum simulations with trapped ions. *Nature Physics*, *8*(4), 277–284.
[5] Houck, A. A., Türeci, H. E., & Koch, J. (2012). On-chip quantum simulation with superconducting circuits. *Nature Physics*, *8*(4), 292–299.
[6] Gross, C., & Bloch, I. (2017). Quantum simulations with ultracold atoms in optical lattices. *Science*, *357*(6355), 995–1001.
[7] Slot, M. R., Gardenier, T. S., Jacobse, P. H., Van Miert, G. C., Kempkes, S. N., Zevenhuizen, S. J., Smith, C. M., Vanmaekelbergh, D., & Swart, I. (2017). Experimental realization and characterization of an electronic Lieb lattice. *Nature Physics*, *13*(7), 672–676.
[8] Singha, A., Gibertini, M., Karmakar, B., Yuan, S., Polini, M., Vignale, G., Katsnelson, M. I., Pinczuk, A., Pfeiffer, L. N., West, K. W., & Pellegrini, V. (2011). Two-dimensional Mott-Hubbard electrons in an artificial honeycomb lattice. *Science*, *332*(6034), 1176–1179.
[9] Georgescu, I. M., Ashhab, S., & Nori, F. (2014). Quantum simulation. *Reviews of Modern Physics*, *86*(1), 153–185.
[10] Fölsch, S., Hyldgaard, P., Koch, R., & Ploog, K. H. (2004). Quantum Confinement in Monatomic Cu Chains on Cu(111). *Physical Review Letters*, *92*(5), 4.
[11] Girovsky, J., Lado, J., Kalff, F., Fahrenfort, E., Peters, L., Fernández-Rossier, J., & Otte, S. (2017). Emergence of quasiparticle Bloch states in artificial crystals crafted atom-by-atom. *SciPost Physics*, *2*(3), 1–12.
[12] Khajetoorians, A. A., Wegner, D., Otte, A. F., & Swart, I. (2019). Creating designer quantum states of matter atom-by-atom. *Nature Reviews Physics*, *1*(12), 703–715.
[13] Gomes, K. K., Mar, W., Ko, W., Guinea, F., & Manoharan, H. C. (2012). Designer Dirac fermions and topological phases in molecular graphene. *Nature*, *483*(7389), 306–310.
[14] Slot, M. R. (2019). *Patterning atomic flatland: Electronic lattices crafted atom by atom* (Doctoral dissertation). Utrecht University, Utrecht.
[15] Fölsch, S., Martínez-Blanco, J., Yang, J., Kanisawa, K., & Erwin, S. C. (2014). Quantum dots with single-atom precision. *Nature Nanotechnology*, *9*(7), 505–508.
[16] Pan, Y., Kanisawa, K., & Fölsch, S. (2017). Creating and probing quantum dot molecules with the scanning tunneling microscope. *Journal of Vacuum Science & Technology B*, *35*(4), 04F102.
[17] Chen, C. J. (2008). *Introduction to Scanning Tunneling Microscopy* (2nd ed.). Oxford, Oxford University Press.
[18] Voigtländer, B. (2015). *Scanning probe microscopy*. Heidelberg, Springer.
[19] Binnig, G., Rohrer, H., Gerber, C., & Weibel, E. (1982). Surface Studies by Scanning Tunneling Microscopy. *Physical Review Letters*, *49*(1), 57–61.
[20] Taguchi, A., & Kanisawa, K. (2006). Stable reconstruction and adsorbates of InAs(1 1 1)A surface. *Applied Surface Science*, *252*(15), 5263–5266.
[21] Yang, J., Nacci, C., Martínez-Blanco, J., Kanisawa, K., & Fölsch, S. (2012). Vertical manipulation of native adatoms on the InAs(111)A surface. *Journal of Physics Condensed Matter*, *24*(35).
[22] Zhang, Z., & Yates, J. T. (2012). Band bending in semiconductors: Chemical and physical consequences at surfaces and interfaces. *Chemical Reviews*, *112*(10), 5520–5551.

[23] Olsson, L., Andersson, C. B., Håkansson, M. C., Kanski, J., Ilver, L., & Karlsson, U. O. (1996). Charge accumulation at InAs surfaces. *Physical Review Letters*, *76*(19), 3626–3629.

[24] Yang, J., Erwin, S. C., Kanisawa, K., Nacci, C., & Fölsch, S. (2011). Emergent multistability in assembled nanostructures. *Nano Letters*, *11*(6), 2486–2489.

[25] Eigler, D. M., & Schweizer, E. K. (1990). Positioning single atoms with a scanning tunnelling microscope. *Nature*, *344*(6266), 524–526.

[26] Stern, A., & Lindner, N. H. (2013). Topological Quantum Computation - From Basic Concepts to First Experiments. *Science*, *339*(6124), 1179–1184.